2023 IEEE International Conference on Robotics and Automation (ICRA 2023)
May 29 - June 2, 2023. London, UK

Dual Robot Collaborative System for Autonomous Venous Access Based on Ultrasound and Bioimpedance Sensing Technology

Maria Koskinopoulou, Alperen Acemoglu, Veronica Penza, Leonardo S. Mattos

Abstract— **Accurate needle insertion is an important task in many medical procedures. This paper studies the case of an autonomous needle insertion system for central venous access, which is a risky and challenging procedure involving the simultaneous manipulation of an ultrasound probe and of a catheterization needle. The goal of this medical operation is to provide access to a deep central vein, which is a key step in cardiovascular treatments or for the administration of drugs and treatments for cancer or infections. Accordingly, in this work we propose an autonomous dual-arm system for central venous access. The system is composed of two Franka robotic arms that are precisely co-registered and collaborate to achieve accurate needle insertion by combining ultrasound and bioimpedance sensing to ensure robust deep vessels visualization and venipuncture detection. The proposed system performance is evaluated on a phantom trainer through experiments simulating the jugular vein access for cardiac catheterization purposes. Quantitative results show the system is able to autonomously scan the area of interest, localize the vein and perform autonomous needle insertion with high accuracy and placement error below 1.7mm, proving the potential of the technology for real clinical use.**

Index Terms— **robotic vascular access, bioimpedance sensing, dual-robot, vessel segmentation, ultrasound-guided.**

I. INTRODUCTION

Precise needle placement is a key operation in many medical procedures such as peripheral catheterization, cardiac endovascular treatments, biopsy and treatment of tumours in soft tissues such as breast, prostate and abdomen [1], [2], [3]. Among them, Central Venous Access (CVA) is a routine procedure typically performed by experienced clinicians under ultrasound or x-ray guidance in a surgical room environment.

CVA is most commonly conducted in three locations: the internal jugular vein, the subclavian vein, and the femoral vein. During such procedure, the clinician is forced to perform a balancing action between inserting the catheterization needle and maintaining proper visualization of the target vessel. Ultrasound-guided access is the standard technique for CVA procedures at medical facilities where an ultrasound machine is available. This largely facilitates the procedure, but requires specifically trained clinicians. This is because the orientations of both the ultrasound probe and the needle are pivotal to achieving adequate visualization of the target vessel and proper venipuncture for catheterization [4]. Therefore, performing the detection and continuous visualization of the target vessel while simultaneously precisely controlling the needle insertion is a challenging operation. Furthermore, real-time feedback to the clinician is limited, as the ultrasound probe only shows one image plane at a time and there is practically no feedback regarding the venipuncture moment.

Accordingly, even with experienced clinicians, there is still a risk for errors and associated complications due to misinterpretations of the ultrasound image or improper orientation between the probe and the needle [5]. Therefore, there is a need for technology that makes ultrasound-guided catheterization procedures easier, more reliable, and safer to perform. To this end, robotic ultrasound-guided needle insertion has appeared in the literature to automate the process and address these major issues [6], [7], [8]. In addition, to ensure realistic and reliable ultrasound imaging, Chi *et al.* proposed a robotic scanning method based on imitation learning [9].

A variety of systems have been developed over the past decades to improve vascular access procedures, ranging from manually-operated assistive systems [10], [11] to autonomous robots for both peripheral or central access [12], [13]. Cheng *et al.* introduced a handheld robotic device for semi-autonomous peripheral catheterization by incorporating for the first time in such application a bioimpedance sensor to the needle tip, enabling instantaneous venipuncture detection and improved needle insertion control [10]. Additionally, Chen *et al.* in [14] used a sensing combination of infrared imaging and ultrasound to approach the same needle insertion control problem. Other works also investigated the use of magnetic resonance imaging (MRI) to visualize soft tissue features such as scars or edema during robotic cardiac catheterization, or exploited its combination with fluoroscopy to improve the visualization [15], [16].

Kojcev *et al.* in [17] proposed a dual robot framework for precise needle placement by integrating a vision-based robot control together with an ultrasound image acquisition algorithm for target localization, registration of preoperative, and intraoperative needle tracking to improve catheterization accuracy. Recently, Brattain *et al.* presented a handheld robotic device for femoral vascular access, namely AI-GUIDE (Artificial Intelligence Guided Ultrasound Interventional Device), capable of directing users with no ultrasound or interventional expertise to catheterize the deep femoral vessels [18]. Both systems are ultrasound-guided but require the supervision of a human.

Compared to the latter, the system presented in this paper proposes the integration of a bioimpedence sensor to the needle end-effector as a final step of the robotic insertion process, which has the potential to enable a fully

This work is partially supported by BRACCO S.p.A.

*All the authors are with the Department of Advanced Robotics (ADVR), Istituto Italiano di Tecnologia, 16163 Genova, Italy.
Email: {maria.koskinopoulou}@iit.it

autonomous operation with accurate venipuncture outcome without requiring visual feedback or human supervision. Accordingly, this work presents a dual robot collaborative system guided by a hybrid sensing system including ultrasound (US), electrical bioimpedance (EBI) sensing, force sensing and 3D vision. It comprises a real-time ultrasound-based target vessel localization and segmentation module, a real-time EBI-based venipuncture detection module, a force-based robot control module, and a 3D vision-based target surface detection module. These are complemented by a co-registration method that allows coordinated control and collaboration between the two robotic arms, effectively enabling the fully autonomous insertion of a catheterization needle into a deep vessel.

The proposed autonomous system locates the target vessel based on a pre-operatively defined region of interest, and uses real-time vision to realize an adaptive trajectory planning that provides safe and quick interactions. The system is quantitatively assessed on a commercial trainer for deep vessel access.

The rest of this paper is organised as follows: Section II describes the integration of the hybrid-guided dual robot system and provides an overview of the workflow pipeline and sub-algorithms used. Section III details the experimental setup, and Section IV summarizes the experimental results. Finally, conclusions and future perspectives are provided in Section V.

II. HYBRID-GUIDED DUAL-ROBOT SYSTEM

A high level workflow of the CVA process is shown in Fig. 1. According to the proposed block diagram, the work pipeline can be summarized as follows:

i The region of interest for CVA is defined by the user.
ii The robot detects the target surface using 3D vision and plans the US scanning trajectory.
iii The robot tries to identify the optimal venous access target by autonomously scanning the planned trajectory using force control, which guarantees a good and consistent contact between the US transducer and the skin. In each position the US probe is tilted and slides on the skin while the US images are processed.
iv When the target vessel is detected, the US probe is oriented to center the vessels and acquire its image in the transverse plane.
v The robotic system calibration is used to compute the desired orientation and insertion depth to puncture the vessel in the defined target location. This information is sent to the second robotic arm to execute the needle insertion action.
vi The needle manipulation robot orients and moves the needle towards the target position while acquiring EBI measurements at the needle tip and obtaining updated target information from the vessel tracking module.
vii The needle robot stops the insertion once venipuncture is detected, completing the operation.

The fundamental components (sub-modules) to accomplish the above steps are described below.

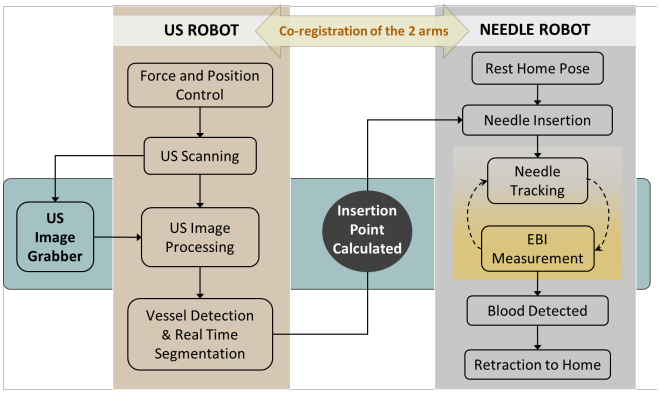

Fig. 1: Dual robotic-arm collaborative system workflow.

A. Co-registration of the robotic arms

The accurate co-registration of the imaging robot and the needle handling robot is an important procedure for the developed system. For this purpose, two custom supports were designed and manufactured: one to hold the ultrasound probe and one for the needle insertion robotic mechanism. In the proof-of-concept setup used in this work, the Cathbot device for peripheral vein catheterization, presented in [10], was modified and adapted to work as the needle insertion end-effector. The control system of this component was kept the same as in the original Cathbot, which was useful also to show that the working principle of Cathbot can indeed be used for fully autonomous operations. Figures 2a and 2b illustrates the two supports and their connections to the Franka robotic arms in a simulation environment.

Hence, to control the two robots, namely Ultrasound Robot $\{R_{us}\}$ and Needle Robot $\{R_n\}$, in a common coordinate system, the Cartesian position that the needle has to reach is computed as:

$$T_{BEn} \cdot T_{EKn} = T^{-1}_{B_{us}B_n} \cdot T_{BEus} \cdot T_{EKus} \tag{1}$$

where $T_{B_{us}Bn}$ is the rigid transformation between the two robotic bases, T_{BEn} and T_{BEus} denote the transformations between the base and the robot's end-effector for the needle and the ultrasound robot respectively, while T_{EKn} and T_{EKus} stands for the relevant transformations between the robots' end-effectors and the printed end-effectors supports. For better understanding, Fig. 2c shows the named individual transformations graphically.

To compute the transformation matrices $T_{B_{us}Bn}$, we follow the calibration procedure described in [19]. Thus, a custom 3D-printed calibration plate, shown in Fig. 3a, was designed to collect the same 3D point on the calibration plate with both robotic platforms $\{R_n\}$ and $\{R_{us}\}$. Doing this, we acquire the unique 3D position of each robotic end-effector (Fig. 3b,c) and the corresponding robot configuration pose, which enable the calculation of the transformations.

The relevant transformations between the needle tip $\{K_{us}\}$ and the ultrasound transducer $\{R_{us}\}$ are derived from the CAD model of each device as a transformation matrix, given in Eq.2-3, including both the relevant rotation between

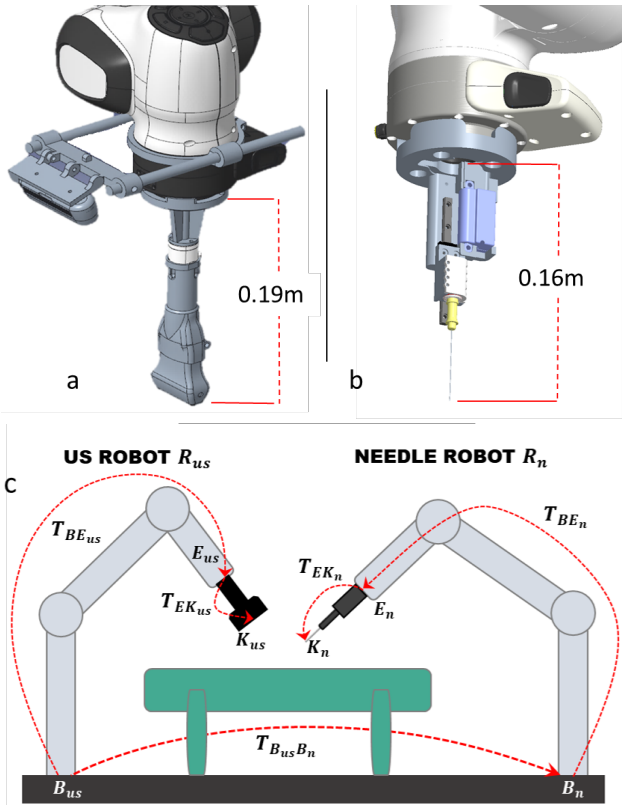

Fig. 2: Co-registration of the dual-robot system; a. design model of the custom made ultrasound probe holder with a total length of 0.19m; b. design model of the custom made needle holder with a total length of 0.16m; c. graphical sketch of the calibration process and depiction of the individual computed transformations.

the robot's end-effector and the attached device. For the ultrasound holder, the rotation on x axis is -15 deg and on y -45 deg, while on z there is no rotation. The needle insertion mechanism does not add rotation components. The given values were also experimentally verified once the system was implemented.

$$T_{EKus} = \begin{pmatrix} 0.70 & 0.09 & -0.69 & 0.03 \\ 0.09 & 0.09 & 0.23 & 0.03 \\ 0.69 & -0.23 & 0.67 & 0.19 \\ 0 & 0 & 0 & 1 \end{pmatrix} \quad (2)$$

$$T_{EKn} = \begin{pmatrix} 1 & 0 & 0 & 0.01 \\ 0 & 1 & 0 & 0 \\ 0 & 0 & 1 & 0.16 \\ 0 & 0 & 0 & 1 \end{pmatrix} \quad (3)$$

This calibration is done in the pre-operative phase and remains fixed and valid for all the experiments since the designed end-effectors and the relevant position between the two robots do not change.

Subsequently, the co-registration of the dual-robot system was evaluated by computing the target positioning error

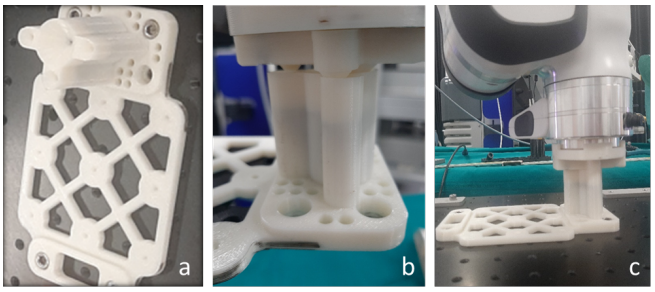

Fig. 3: Two-robots calibration procedure: a. custom 3d-printed calibration plate with a unique attachment for the Franka end-effector. b. Franka approaches the unique position. c. Perfect attachment between Franka and calibration plate.

guiding the needle tip to a set of known points pointed by the ultrasound probe holder as illustrated in Fig. 4. Hence, we first place the ultrasound robot on a set of N=16 predefined positions on top of a tissue phantom and then asked the needle robot to reach the same point p_i each time using the derived transformation equation. The acquisition was repeated 16 times and the error was computed as:

$$RMSE_{usr} = \sqrt{\frac{\sum_1^N (p_i^{us} - p_i^n)^2}{N}} \quad (4)$$

where p_i^n are the points measured with the needle tip, p_i^{us} are the known points in the ultrasound robot coordinate system. This resulted in a calibration error of $1.47mm$.

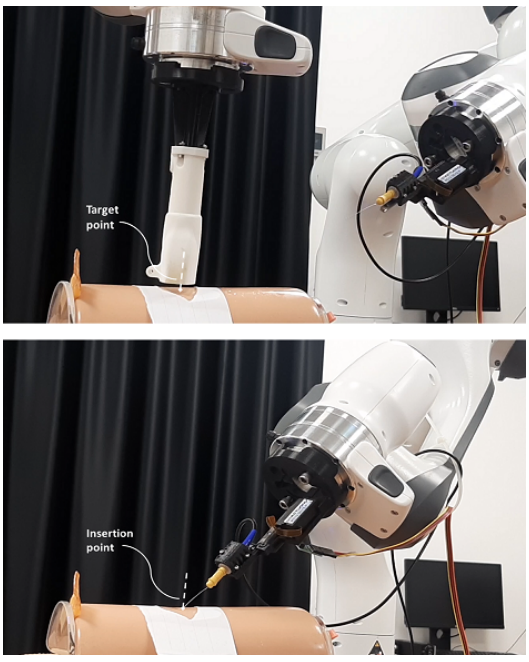

Fig. 4: Calibration process verification.

B. Ultrasound image registration

The purpose of US image calibration is to establish the correspondence between the world frame and the US image

frame. To do so, we followed the method proposed by Li et al. in [20]. According to this, a calibration sphere of 3mm radius was printed and placed in a fixed position in the center of a hand-made agarose tissue model that permits ultrasound visualization. Then, to realize the autonomous ultrasound image calibration procedure, a scanning trajectory was defined and executed on the surface of the tissue model to cover the whole phantom area. To acquire enough images, the scanning translation step was set to 10mm with a velocity of 0.2m/s. In addition, a rotation of 30deg around each recorded position was performed with a rotational velocity of 0.1 rad/s. This data allowed computing the transformation from the robot's coordinates to the US image ones as a mapping between the two systems.

The resulting ultrasound image registration was evaluated in an analogous manner with the procedure followed to evaluate the two robot calibration system. The process was repeated 10 times and the computed error was 1.44mm ($\bar{std} = 0.61mm$).

C. Ultrasound vessel localization and segmentation module

To perform real time detection of deep vessels, a segmentation algorithm based on the well-known Mask Regional Convolutional Neural Network (Mask R-CNN) implementation [21] was used. Mask R-CNN provides a scalable means for instance segmentation and classification of objects by detecting at the same time the bounding box, the mask and the class of each instance. The training process presupposes the acquisition of a well-constructed dataset annotated with the mask of the structure of interest. The Mask R-CNN architecture includes a CNN backbone, a region proposal network, and a ROI Align layer. The "box head" is a series of fully connected layers that outputs the predicted class and bounding box for each object. The "mask head" outputs binary segmentation masks for each object instance.

The training of our Mask R-CNN implementation was performed on a total of 1066 images derived form a publicly available dataset [22], which were acquired using two different ultrasound devices (Ultrasonix and Toshiba). Here, this dataset was further enhanced with a set of images from the jugular veins of the authors acquired with our own ultrasound machine (GE Healthcare Venue Go™). The images were coupled with labeling data describing the positions and sizes of the vessel instances (as shown in Fig. 5). This data was then used to design the evolutionary cascade and to create training images of 24×24 pixels in size.

D. EBI-guided needle insertion

This system module exploits a venous entry detection system based on electrical impedance sensing developed in previous works [10], [23], which showed that different types of tissues present different electrical impedance values. Accordingly, a concentric bipolar needle electrode F8990/65 (FIAB SpA, Florence, Italy) measuring $65mm \times 0.45mm$ was placed on the robotic needle holder to measure the impedance values at its tip.

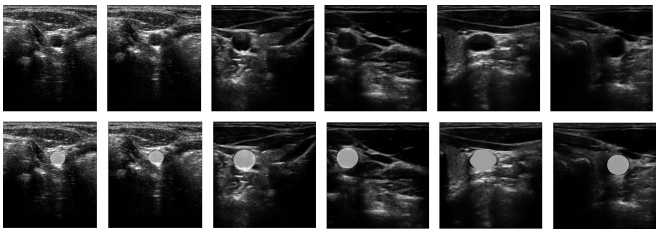

Fig. 5: Training sample pair images. Top row: original ones; Bottom row: annotated images where the white circles depicts the annotated vessel mask.

A Robot Operating System (ROS) framework implementation was developed to establish the communication between the EBI control box and the other catheterization system components. The integrated EBI control box was based on the microcontroller Atmega328 (Atmel Co., California, U.S.), which was configured to send a set of commands to the master PC through the established ROS communication using the PySerial library. The commands involved tasks for: (i) reading the EBI measurement from the needle tip in a continuous loop with a sampling frequency of $50Hz$; (ii) checking for the impedance value of blood and (iii) stopping the injection actuator when blood is detected.

III. EXPERIMENTAL SETUP

A realistic central venous access scenario was established for experimental assessment of the developed system, as shown in Fig. 6. Experiments were based on an echolucent phantom trainer (Limbs & Things LTD, UK) designed for training in US-guide deep vein catheterizations. The phantom's dimensions are $100mm \times 190mm$ and includes an embedded vein with $2.0mm$ in diameter. The vein is self sealing for repeated uses and can be filled with blood analogue liquid. In this work, we filled the vein with knee aspirant fluid (Part No 70022, Limbs & Things LTD, UK), which provides good contrast for US visualization and presents an impedance range that enables the use of our EBI sensor.

The setup also included two Franka robots (Franka Emika GmbH, Germany), a Venue Go™ high-frequency ultrasound machine (GE Healthcare, USA) with a linear transducer (model: 12L-RS), a Nano25 force/torque sensor (ATI, USA), a D435i RealSense RGBD camera (Intel, USA), and the adapted Cathbot device as described previously.

A workstation computer with a CPU Intel i7-4820K with four cores and hyper-threading (eight virtual cores) was used for the integration and management of the different system components. It included a NVIDIA GTX 1050Ti (4GB) graphics card and a Magewell Pro Capture AIO 4k video grabber card. In addition, it was configure to run Ubuntu 18.04.6 LTS (Bionic Beaver) and the ROS 1, Melodic distribution. This workstation was used to control the two robotic arms, acquire data from the RGBD camera and F/T sensors, acquire and process US images for vein visualization and detection, collect EBI measurements, and control the embedded Cathbot device.

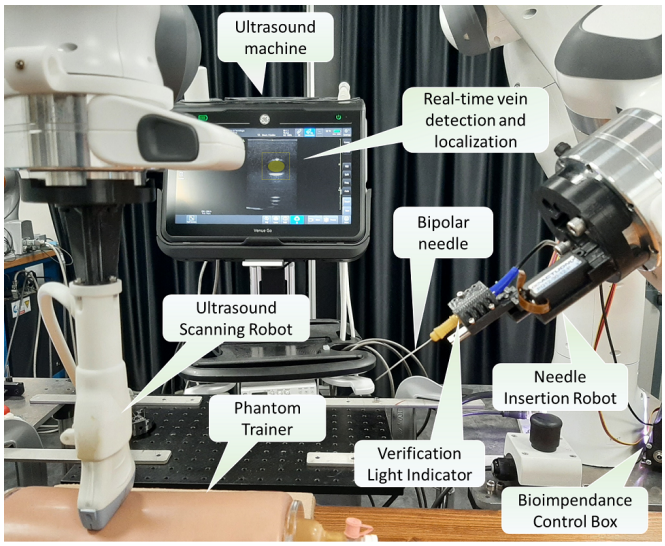

Fig. 6: Experimental setup of the hybrid-guided dual-arm autonomous system for central venous access.

IV. EXPERIMENTAL RESULTS

The assessment of the ultrasound vessel segmentation module was based on 600 test images randomly selected from the dataset. The performance metric used was the Intersection over Union (IoU) between the segmented masks and the available ground-truth segmentation. Illustrative snapshots are shown in Fig.7.

The derived results are summarized in Table I where values for the *accuracy*, *precision*, *recall* and *F-score* metrics are given for three different IoU thresholds (0.2, 0.5 and 0.8). According to these results, the accuracy level of our Mask RCNN model ranges from 0.91 to 0.96, demonstrating a high overall performance.

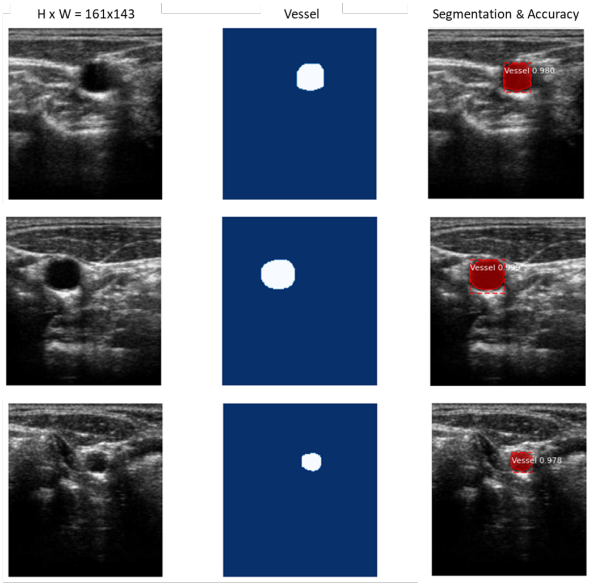

Fig. 7: Snapshots from the experimental assessment of the US vessel detection and segmentation module.

TABLE I: Mask RCNN deep-vessel segmentation evaluation

Threshold	20%	50%	80%
Accuracy	0.96	0.94	0.91
Precision	0.98	0.98	0.97
Recall	0.99	0.96	0.94
F-score	0.98	0.97	0.95

The venous access process described in Sec. II was repeated 60 times, with the robots starting from 12 different points and considering 12 different access points in the phantom's vein. This means that for each starting point, the computed trajectories were repeated 5 times. The trajectories of the Needle Robot are presented in Fig.8a with different colors. The standard deviation of the 5 iterations is shown as a lighter shadow. The pink curved plane in the plot represents the phantom surface. Additionally, three indicative snapshots from one experimental execution are given in Fig.8b,c,d, while an illustrative video of the experimental process can be found at this link: `https://youtu.be/cDZK2Ce_dgk`.

The mean 3D RMS error of the total 60 trials was measured as the difference between the insertion point on the skin (defined as a projection of the needle insertion trajectory computed based on information from the Ultrasound Robot) and the actual insertion point reached by the needle tip. This resulted in a positioning RMS error of $1.71mm$ ($\bar{std}$ $0.52mm$), which can be considered as the accuracy of the system. In terms of the orientation during insertion, the mean rotation error measured over the 60 iterations was $4deg$, while the mean resultant insertion angle was $42deg$ with respect to the reference plane of the ultrasound transducer. It is worth noting that the EBI sensor module worked perfectly during all trials, which was attested by confirming the needle tip was correctly positioned inside the target vessel upon completion of the insertion procedure.

V. CONCLUSIONS

The developed dual robotic-arm collaborative system successfully demonstrated autonomous central venous access on a realistic phantom model. This shows that real-time data from the hybrid sensing system based on ultrasound, bioimpedance, force and 3D vision could be effectively used by the intelligent control algorithms to enable the accurate autonomous execution of this challenging medical procedure.

To the best of our knowledge, this is the first time a bioimpedance sensor is combined with ultrasound imaging to perform autonomous CVA. This integration of EBI sensing has large potential to enable safer needle insertion control by providing robust feedback on the venipuncture action. In addition, it can contribute to improve the success rate of difficult catheterizations, such as those performed on small vessels. Moreover, EBI sensing can partially compensate targeting errors arising from the robotic systems' co-registration method. This could be observed during the experiments given the system was able to successfully perform venous access attempts despite the positioning RMS error of 1.71mm.

In the future, we plan to test the system on a custom phantom that simulates the deep vessels of the upper leg

containing both artery and vein to address the discrimination between them during the CVA task. Trials on animals are also considered for the near future. These future trials will involve clinicians to assess the usability and utility of the system from a clinical point of view. Finally, a graphical user interface (GUI) shall be designed to facilitate the use of the system and allow for user supervision during the operations.

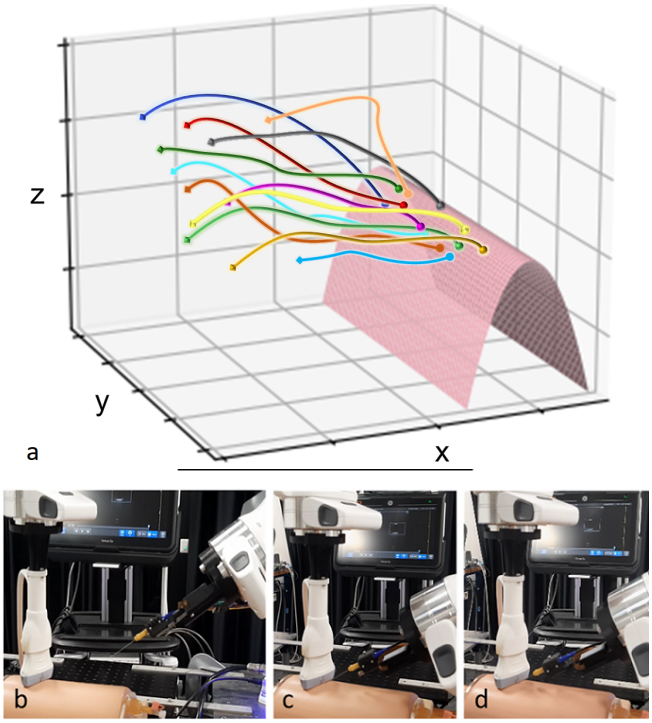

Fig. 8: a. Plot of the 3D trajectories performed to evaluate the system. Each trajectory is marked with different color. A lighter shadow of each color gives the standard deviation values. The curved 3D plane depicts the phantom model. Indicative snapshot from the experiments are shown in the second row where in b. the Needle Robot moves towards the target, c. target position reached, d. needle insertion is performed.

REFERENCES

[1] Z. Cheng, B. L. Davies, D. G. Caldwell, G. Barresi, Q. Xu, and L. S. Mattos, "A hand-held robotic device for peripheral intravenous catheterization," *Proceedings of the Institution of Mechanical Engineers, Part H: Journal of Engineering in Medicine*, vol. 231, no. 12, pp. 1165–1177, 2017.

[2] K. Liang, A. J. Rogers, E. D. Light, D. von Allmen, and S. W. Smith, "Three-dimensional ultrasound guidance of autonomous robotic breast biopsy: feasibility study." *Ultrasound in medicine & biology*, vol. 36 1, pp. 173–7, 2010.

[3] F. J. Siepel, B. M. Maris, M. K. Welleweerd, V. Groenhuis, P. Fiorini, and S. Stramigioli, "Needle and biopsy robots: a review," *Current Robotics Reports, Springer*, 2021.

[4] L. J. Brattain, C. Floryan, O. P. Hauser, M. Nguyen, R. J. Yong, S. B. Kesner, S. B. Corn, and C. J. Walsh, "Simple and effective ultrasound needle guidance system," *2011 Ann. Intern. Conf. IEEE Engineering in Medicine and Biology Society*, pp. 8090–8093, 2011.

[5] K. Li, Y. Xu, and M. Q.-H. Meng, "An overview of systems and techniques for autonomous robotic ultrasound acquisitions," *IEEE Transactions on Medical Robotics and Bionics*, vol. 3, no. 2, pp. 510–524, 2021.

[6] Y. Kobayashi, J. Hong, R. Hamano, K. Okada, M. G. Fujie, and M. Hashizume, "Development of a needle insertion manipulator for central venous catheterization," *The international journal of medical robotics and computer assisted surgery: MRCAS*, vol. 8, no. 1, p. 34—44, March 2012. [Online]. Available: https://doi.org/10.1002/rcs.420

[7] S. Chen, F. Wang, Y. Lin, Q. Shi, and Y. Wang, "Ultrasound-guided needle insertion robotic system for percutaneous puncture," *International Journal of Computer Assisted Radiology and Surgery*, vol. 16, pp. 475 – 484, 2021.

[8] M. Ikhsan, K. Tan, and A. Putra, "Assistive technology for ultrasound-guided central venous catheter placement," *Journal of Medical Ultrasonics*, vol. 45, 04 2017.

[9] W. Chi, G. Dagnino, T. M. Y. Kwok, A. Nguyen, D. Kundrat, M. E. M. K. Abdelaziz, C. Riga, C. Bicknell, and G.-Z. Yang, "Collaborative robot-assisted endovascular catheterization with generative adversarial imitation learning," in *2020 IEEE International Conference on Robotics and Automation (ICRA)*, 2020, pp. 2414–2420.

[10] Z. Cheng, B. L. Davies, D. G. Caldwell, and L. S. Mattos, "A hand-held robot for precise and safe pivc," *IEEE Robotics and Automation Letters*, vol. 4, no. 2, pp. 655–661, 2019.

[11] D. Auyong, S. Yuan, A. Rymer, C. Green, and N. A. Hanson, "A randomized crossover study comparing a novel needle guidance technology for simulated internal jugular vein cannulation," *Anesthesiology*, vol. 123, p. 535–541, 2015.

[12] N. Zevallos, E. Harber, Abhimanyu, K. Patel, Y. Gu, K. Sladick, F. Guyette, L. Weiss, M. R. Pinsky, H. Gomez, J. Galeotti, and H. Choset, "Toward robotically automated femoral vascular access," in *2021 Intern. Symp. on Medical Robotics (ISMR)*, 2021, pp. 1–7.

[13] G. Fagogenis, M. Mencattelli, Z. Machaidze, B. Rosa, K. Price, F. Wu, V. Weixler, M. Saeed, J. E. Mayer, and P. E. Dupont, "Autonomous robotic intracardiac catheter navigation using haptic vision," *Science Robotics*, vol. 4, no. 29, p. eaaw1977, 2019.

[14] A. I. Chen, M. L. Balter, T. J. Maguire, and M. L. Yarmush, "Deep learning robotic guidance for autonomous vascular access," *Nature Machine Intelligence*, vol. 2, no. 2, pp. 104–115, 2020.

[15] K.-H. Lee, K. C. D. Fu, Z. Guo, Z. Dong, M. C. W. Leong, C.-L. Cheung, A. P.-W. Lee, W. Luk, and K.-W. Kwok, "Mr safe robotic manipulator for mri-guided intracardiac catheterization," *IEEE/ASME Transactions on Mechatronics*, vol. 23, no. 2, pp. 586–595, 2018.

[16] M. E. M. K. Abdelaziz, D. Kundrat, M. Pupillo, G. Dagnino, T. M. Y. Kwok, W. Chi, V. Groenhuis, F. J. Siepel, C. Riga, S. Stramigioli, and G.-Z. Yang, "Toward a versatile robotic platform for fluoroscopy and mri-guided endovascular interventions: A pre-clinical study," in *2019 IEEE/RSJ International Conference on Intelligent Robots and Systems (IROS)*, 2019, pp. 5411–5418.

[17] R. Kojcev, B. Fuerst, O. Zettinig, J. Fotouhi, S. C. Lee, B. Frisch, R. H. Taylor, E. Sinibaldi, and N. Navab, "Dual-robot ultrasound-guided needle placement: closing the planning-imaging-action loop," *International Journal of Computer Assisted Radiology and Surgery*, vol. 11, pp. 1173–1181, 2016.

[18] L. Brattain *et al.*, "Ai-enabled, ultrasound-guided handheld robotic device for femoral vascular access," *Biosensors*, vol. 11 (12), p. 522, 18 Dec. 2021.

[19] V. Penza, Z. Cheng, M. Koskinopoulou, A. Acemoglu, D. G. Caldwell, and L. S. Mattos, "Vision-guided autonomous robotic electrical bio-impedance scanning system for abnormal tissue detection," *IEEE Transactions on Medical Robotics and Bionics*, vol. 3, no. 4, pp. 866–877, 2021.

[20] R. Li, K. Niu, and E. V. Poorten, "A framework for fast automatic robot ultrasound calibration," in *2021 International Symposium on Medical Robotics (ISMR)*, 2021, pp. 1–7.

[21] W. Abdulla, "Mask r-cnn for object detection and instance segmentation on keras and tensorflow," https://github.com/matterport/MaskRCNN, 2017.

[22] R. Benes, J. Karasek, R. Burget, and K. Riha, "Automatically designed machine vision system for the localization of cca transverse section in ultrasound images," *Comput. Methods Prog. Biomed.*, vol. 109, no. 1, p. 92–103, jan 2013. [Online]. Available: https://doi.org/10.1016/j.cmpb.2012.08.014

[23] Z. Cheng, D. Dall'Alba, S. Foti, A. Mariani, T. Chupin, D. G. Caldwell, G. Ferrigno, E. De Momi, L. S. Mattos, and P. Fiorini, "Design and Integration of Electrical Bio-impedance Sensing in Surgical Robotic Tools for Tissue Identification and Display," *Frontiers in Robotics and AI*, vol. 6, 2019.